ENVIRONMENTAL RESEARCH
LETTERS

LETTER • OPEN ACCESS

Physically based equation representing the forcing-driven precipitation in climate models

To cite this article: Donghyun Lee *et al* 2023 *Environ. Res. Lett.* **18** 094063

ENVIRONMENTAL RESEARCH
LETTERS

LETTER

Physically based equation representing the forcing-driven precipitation in climate models

Donghyun Lee[1,*], **Sarah N Sparrow**[2], **Seung-Ki Min**[3], **Sang-Wook Yeh**[4] and **Myles R Allen**[1,5]

[1] Environmental Change Institute, School of Geography and the Environment, University of Oxford, Oxford, United Kingdom
[2] Oxford e-Research Centre, Department of Engineering Science, University of Oxford, Oxford, United Kingdom
[3] Division of Environmental Science and Engineering, Pohang University of Science and Technology, Pohang, Republic of Korea
[4] Department of Marine Science and Convergent Engineering, Hanyang University, Ansan, Republic of Korea
[5] Atmospheric Oceanic and Planetary Physics, Department of Physics, University of Oxford, Oxford, United Kingdom
* Author to whom any correspondence should be addressed.

E-mail: donghyun.lee@ouce.ox.ac.uk

Keywords: precipitation change, atmospheric energy budget, simulation uncertainty, the Paris Agreement, mitigation pathways

Supplementary material for this article is available online

OPEN ACCESS

RECEIVED
11 May 2023

REVISED
24 August 2023

ACCEPTED FOR PUBLICATION
30 August 2023

PUBLISHED
19 September 2023

Abstract

This study aims to improve our understanding of the response of precipitation to forcings by proposing a physically-based equation that resolves simulated precipitation based on the atmospheric energy budget. The equation considers the balance between latent heat release by precipitation and the sum of the slow response by tropospheric temperature changes and the fast response by abrupt radiative forcing (RF) changes. The equation is tuned with three parameters for each climate model and then adequately reproduces time-varying precipitation. By decomposing the equation, we highlight the slow response as the largest contributor to forcing-driven responses and uncertainty sizes in simulations. The second largest one to uncertainty is the fast-RF response from aerosols or greenhouse gases (GHG), depending on the low or highest Coupled Model Intercomparison Projection 6 future scenarios. The likely range of precipitation change at specific warming levels under GHG removal (GGR) and solar radiation management (SRM) mitigation plans is evaluated by a simple model optimizing the relationship between temperature and decomposed contributions from multi-simulations under three scenarios. The results indicate that GGR has more severe effects from aerosols than GHG for a 1.5 K warming, resulting in 0.91%–1.62% increases in precipitation. In contrast, SRM pathways project much drier conditions than GGR results due to the tropospheric cooling and remaining anthropogenic radiative heating. Overall, the proposed physically-based equation, the decomposition analysis, and our simple model provide valuable insights into the uncertainties under different forcings and mitigation pathways, highlighting the importance of slow and fast responses to human-induced forcings in shaping future precipitation changes.

1. Introduction

Precipitation is a fundamental component of the Earth's climate system, responsible for regulating the distribution of water and energy across the atmosphere, oceans, and land (Bengtsson 2010, Gleeson *et al* 2020). Within the hydrological cycle, liquid water evaporates from the ground and remains in the atmosphere as water vapor. It forms clouds and eventually returns to the surface as precipitation. This process involves the exchange of energy, with evaporation absorbing the surrounding energy from the surface and condensation releasing it into the atmosphere. Water vapor acts as both a forcing (Kondratev 1972) and a response to the external forcings due to its temperature-dependent relationship with the Clausius-Clapeyron relationship (Held and Soden 2006). Changes in this hydrological cycle have critical impacts on extreme climate risks (Paik *et al* 2020), water resources for

human use (Kundzewicz and Döll 2009), agricultural production (Hirabayashi *et al* 2013), and ecosystems (Walther *et al* 2002).

Previous studies have examined the precipitation variation by analyzing the general circulation model (GCM) involved in the Coupled Model Intercomparison Projection (CMIP). Globally averaged outputs of GCMs are examined to generalize the precipitation response to the forcings. Without forcing variations, this precipitation can be controlled by the temperature, known as hydrological sensitivity (HS), showing 2–3%/K (Allen and Ingram 2002, Pendergas 2020). Unlike the counterfactual conditions of HS, the world perpetually interacts with external forcings, and the atmospheric energy balance is perturbed and adjusted even on a short-term scale. The actual changes in precipitation are affected by HS and instantaneous radiative forcing (RF). The forcing-driven changes in precipitation are diverse depending on the types of GCMs and amount of external forcings (Fläschner *et al* 2016, Samset *et al* 2016).

After the Paris Agreement, global warming mitigation is promised. The mitigation plans must be determined based on the latest scientific understanding of forcing-driven impacts on possible approaches, like GHG removal (GGR) or solar radiation management (SRM). Some previous studies examined the precipitation change under GGR or SRM pathways. For examples, Sanderson *et al* (2017) used a single GCM to achieve a 1.5 and 2.0 K stable climate at the end of the 21st century under GGR methods, showing more increase in precipitation under warmer conditions. Laakso *et al* (2020) used two GCMs under GGR and SRM approaches, showing much drier conditions in SRM relative to GGR. However, high computational resources for simulations limit GCM numbers to explore the difference between GGR and SRM and hinder the robustness of their findings.

A reduced-complexity emulator for precipitation is the countermeasure to investigate possible changes under the given forcing conditions. Only a few studies examined the time-varying precipitation with a numerical equation. Shine *et al* (2015) proposed a conceptual model based on the impulse response functions but their parameters are theoretical values. Richardson *et al* (2018) considered the CO_2 and non-CO_2 together, but their parameters are estimated in averaged sense from limited numbers of GCMs. MacMartin *et al* (2018) developed an integrated equation but only considered the CO_2 and SRM. Laakso *et al* (2020) proposed an equation that captured the GGR and SRM in two GCMs, but its non-CO_2 part is empirical. Yeh *et al* (2021) introduced the integrated time-varying equation in a simplified form. However, the equation is designed for a single GCM and only applicable to CO_2-forcing conditions. Given the wide range of uncertainty in precipitation among GCMs, there is a need to improve the time-varying numerical equation to capture the diverse characteristics of multiple GCMs and include physically missed fast responses driven by RF of non-CO_2 GHG and aerosols.

This study suggests an equation that resolves the global mean precipitation change at given forcing conditions. This equation physically explains the precipitation variation and quantifies the uncertainty sources. Finally, we evaluate reliable ranges of precipitation changes with a model based on the statistically optimized functions and compare the differences between GGR and SRM approaches. This paper is structured as follows. Section 2 describes model and analysis methods, including the definition of the equation resolving precipitation responses, three parameters indicating model sensitivity, and the uncertainty among GCMs. Results are provided in section 3 for evaluating our equation, quantifying the size of contributions to the precipitation variations and uncertainty among GCMs, and estimating the likely ranges of precipitation change under mitigation pathways. Section 4 gives a summary and discussion.

2. Data and methods

2.1. Data

To check the universal application of our equation, we mainly focus on climate experiments shared by many GCMs. We use simulations participating in the CMIP Phase 6 (CMIP6) project on the condition that GCMs integrate all four experiments: piControl, abrupt-4xCO2, 1pctCO2, and historical. We have 55 GCMs and describe their details in table S1. We also examine 14 GCMs having hist-GHG, hist-nat and hist-aer simulations to assess the precipitation responses under each group of climate forcing. For future analysis, we select 40 GCMs having all simulations under the three Shared Socioeconomic Pathways (SSP) scenarios (table S1). For the reference values of concentration and effective RF of scenarios, we use the single protocol dataset of the Reduced Complexity Model Intercomparison Project (RCMIP, Nicholls *et al* 2020). Additionally, CMIP6 GCM having SSP1-1.9 or SRM simulations (G6solar) are examined to validate our findings (table S1). SSP1-1.9 is the ambitious mitigation scenario comparable to the 1.5 K warming levels (e.g. Kriegler *et al* 2018). G6solar scenario controls the solar constant to reduce the SSP5-8.5 scenarios to reach the global warming levels of SSP2-4.5 (Visioni *et al* 2021, 2023). Notably, we calculate the individual model results and then average them for the multi-model ensemble (MME) mean. To test any bias due to dependency among GCM members (Abramowitltz *et al* 2019), we quantify the model dependency effects (check details in figure S1). All possible MME candidates proved insignificant differences. Therefore, our results are globally averaged,

including ocean and land areas, and MME covers all available GCMs.

2.2. Precipitation equation

We build a physically based equation to emulate precipitation variation. Here, the emulation implies the computed precipitation according to the equation. Allen and Ingram (2002) introduced the straightforward concept of precipitation change with atmospheric energy variation. The hydrological response is balanced not by the thermodynamic responses of moisture but by the availability of atmospheric energy. The energy budget equation of the troposphere in the transient phase can be written as follows:

$$\Delta P \approx \alpha \cdot \Delta T + (\Delta R_C + k \cdot F_s)/L. \quad (1)$$

α is HS parameter, and ΔT is the changes in surface temperature. This first term ($\alpha \cdot \Delta T$) illustrates radiative cooling due to tropospheric warming, called HS effects or slow response (SLOW). R_C is another radiative cooling from tropospheric RF, independent of temperature changes. F_S is the net heat flux into the oceans in the transient, and this transient energy imbalance is scaled by model-dependent K. L is approximately 1 $W \cdot m^{-2}$ for a 1% precipitation increase. This second term represents the RF response in changing forcing conditions, known as the fast response (FAST). Yeh *et al* (2021) further simplify equation (1):

$$\Delta P \approx \alpha \cdot \Delta T - (\beta/L) \cdot \Delta F_{CO_2} \quad (2)$$

$$\Delta F_{CO_2} \approx 5.35 \cdot \ln(C/C_0). \quad (3)$$

The term $(\Delta R_C + k \cdot F_S)/L$ in equation (1) is replaced by $-(\beta/L) \cdot \Delta F_{CO_2}$, implying the fraction (β) of CO_2 RF (ΔF_{CO_2}), and this can be simplified by using equation (3) of Myhre *et al* (1998) explaining RF as the expression of CO_2 concentration (C) change relative to the base level of it (C_0). This number explains the fraction of CO_2 RF that reheats the atmosphere, also known as the fast CO_2 response ($FAST_{CO_2}$), eventually inhibiting latent heat releases. Although Allen and Ingram (2002) and Yeh *et al* (2021) explained well the precipitation changes under the transient forcing conditions, those equations only explain the precipitation changes driven by CO_2.

First, our study expands equation (2) to reflect the GHG effects beyond Yeh *et al* (2021) approach.

$$\Delta P \approx \alpha \cdot \Delta T - (\beta/L) \cdot \Delta F_{GHG}. \quad (4)$$

Equation (4) shares most of the terms in equation (2) except for the atmospheric RF amount (ΔF). Although the previous study follows Myhre *et al* (1998), here we chose the approach of Etminan *et al* (2016) because they proved a better performance than Myhre *et al* (1998). The atmospheric RF equations for the first three major components of GHGs: CO_2 (ΔF_{CO_2}), CH_4 (ΔF_{CH4}), and N_2O (ΔF_{N2O}) are

$$\Delta F_{CO_2} \approx [5.36 + f_C^*(C, N)] \times \ln(C/C_0) \quad (5)$$

$$\Delta F_{CH_4} \approx [0.043 + f_M^*(M, N)] \times \left(\sqrt{M} - \sqrt{M_0}\right) \quad (6)$$

$$\Delta F_{N_2O} \approx [0.117 + f_N^*(C, N, M)] \times \left(\sqrt{N} - \sqrt{N_0}\right). \quad (7)$$

Those expressions (equations (5)–(7)) are adopted from Etminan *et al* (2016) and written in concise format. Please note that M and N indicate the concentration of CH_4 and N_2O, and M_0 and N_0 show their base climate level. For the time-varying functions of concentration in the left term (f_C^*, f_M^*, and f_N^*), we describe their full expression in table S2. Consequently, the total sum of atmospheric RF from GHG components (ΔF_{GHG}) is

$$\Delta F_{GHG} \approx \Delta F_{CO_2} + \Delta F_{CH_4} + \Delta F_{N_2O}. \quad (8)$$

In equation (8), ΔF_{GHG} is explained mainly by three dominant components. Since other well-mixed GHG components may have effects in the recent decade (1950–2020), we check their potential effects by adopting the Priestley-Center data (Smith 2020), which evaluated various effective RF of CMIP6 simulations. As the effective RF values are likely around RF values (Lee *et al* 2021), we test the effects of other well-mixed GHG by adding their effective RF values as the RF on equation (8). Eventually, we represent the GHG RF by simply equation (8) because emulations of hist-GHG perform better without their effects (figure S2(E)).

After reflecting on the fast response of GHG ($FAST_{GHG}$) to equation (4), we introduce a new term to reflect the effects of aerosols. Since aerosols-induced shortwave impacts change tropospheric temperature and they are reflected in SLOW by definition, we only consider the RF response to the precipitation independent of the temperature variation ($FAST_{Aerosols}$). $FAST_{Aerosols}$ is comparable to the net amount of longwave radiation in the atmosphere and sensible heat flux from the atmosphere to the surface (e.g. Zhou and Savijärvi 2014, Richardson *et al* 2016, Myhre *et al* 2018, Zhang *et al* 2021). Thus, equation (4) is now updated:

$$\Delta P \approx \alpha \cdot \Delta T - (\beta/L) \cdot \Delta F_{GHG} + (\gamma/L) \cdot \Delta F_{Aerosols}. \quad (9)$$

The $FAST_{Aerosols}$, $(\gamma/L) \cdot \Delta F_{Aerosols}$, is expressed by the scaled coefficient parameter (γ) multiplied by the RF in the third term ($\Delta F_{Aerosols}$). We adopt the evaluated effective RF values (Smith 2020) to

account for $\Delta F_{\text{Aerosols}}$. Since model estimated longwave radiation amount caused by aerosols are highly uncertain for both aerosol-radiation interactions and aerosol-cloud interactions (Zelinka *et al* 2014, Smith *et al* 2020, 2021), here we introduce the model-dependent parameter γ indicating the residual atmospheric remained RF scaled from the effective RF values (e.g. Lee *et al* 2021). Positive γ implies a further decrease in precipitation under the rising aerosols concentration.

2.3. Three parameters of models

Three parameters illustrate the model sensitivity to the temperature and RF of GHG and aerosols. The parameter α is estimated by the regression slope between temperature and precipitation from the simulation of abrupt-4xCO2 (figure S2(A)), excluding the first 20 years to escape unresolved feedback effects from abrupt changing of forcing (Andrews *et al* 2015). The parameter β is measured from 1pctCO2 by the scale factor based on equation (2) (figure S2(B)). For the parameter γ, we first test the direct measurement from 14 GCMs with hist-aer simulations. After that, we estimate the γ indirectly from all forcing simulations by relocating equation (9) ($\text{FAST}_{\text{Aerosols}} \approx \Delta\text{P} - \text{SLOW} - \text{FAST}_{\text{GHG}}$). Since forcing conditions are unlike abrupt-4xCO2, we use the entire periods of simulations to estimate parameters β and γ to acquire stability under the transient forcing conditions (Rugenstein *et al* 2020). We confirm the indistinctive differences between MME mean results of direct and indirect γ (figure S2(F)). Since we also find a significant correlation between them ($r = 0.80$), all of our main results use the indirect γ, having more GCM numbers.

2.4. Quantification of uncertainty sources

Since precipitation change uncertainty over the globe and the majority of sub-regions is dominantly driven by the model uncertainty rather than internal variability or scenario uncertainty (e.g. Hawkins and Sutton 2011, Nguyen *et al* 2018, Lehner *et al* 2020), this study focuses on the model uncertainty which is measured by the variance (Var) utilizing the mean function (E in equation (10)).

$$\text{Var}(\Delta P) = E\left(\Delta \text{P}^2\right) - [E(\Delta P)]^2. \tag{10}$$

Arithmetically, the uncertainty size can be decomposed by three different terms having four variables. Please note that we use the single timeseries of RF (Etminan *et al* 2016), and effective RF (Smith 2020) for all GCMs. First, we simplified equation (9) as below:

$$\Delta P \approx a \cdot b + c + d. \tag{11}$$

The letters *a, b, c,* and *d* indicate each model's variables of HS parameter α, temperature changes (ΔT), FAST_{GHG}, and $\text{FAST}_{\text{Aerosols}}$. With this equation (11), model uncertainty can be written by

$$\begin{aligned}\text{Var}(\Delta P) = {} & \text{Var}(ab) + \text{Var}(c) + \text{Var}(d) + 2 \cdot \text{Cov}(ab, c) \\ & + 2 \cdot \text{Cov}(ab, d) + 2 \cdot \text{Cov}(c, d).\end{aligned} \tag{12}$$

Equation (12) explains the model uncertainty by the sum of variance (SV) from a single variable (main effect) and covariance (Cov) from multiple variables (Interactions). The first term Var(ab) can be decomposed.

$$\begin{aligned}&\text{Cov}\left(a^2, b^2\right) + \text{Var}(a) \cdot \text{Var}(b) + \text{Var}(a) \cdot E(b)^2 \\ &+ \text{Var}(b) \cdot E(a)^2 - \text{Cov}(a, b)^2 - 2 \cdot \text{Cov}(a, b) \cdot E(a) \cdot E(b).\end{aligned} \tag{13}$$

In equation (13), the size of Var(a)·Var(b) has a negligible contribution (figure S3). When we exclude the Cov, all the contributors to the uncertainty are always positive and additive. Therefore, we can calculate the percentage uncertainty from these main variables (e.g. Hawkins and Sutton 2009, 2011, Yip *et al* 2011, Lehner *et al* 2020, Lee *et al* 2023).

$$\text{Var}(\Delta P) = \text{SV} + \text{Interactions} \tag{14}$$

$$\text{SV} = \text{Var}(a) \cdot [E(b)]^2 + \text{Var}(b) \cdot [E(a)]^2 + \text{Var}(c) + \text{Var}(d). \tag{15}$$

Eventually, equation (15) quantifies the contributions from various components. From left to right, the uncertainties in HS parameter (SLOW α), in temperature (SLOW ΔT), FAST_{GHG} (sum of $\text{FAST}_{\text{CO}_2}$, FAST_{CH4}, and FAST_{N2O},), and $\text{FAST}_{\text{Aerosols}}$, respectively. Check figure S3 for the quantified size details.

3. Results

3.1. Evaluation for physically based equation

Forcing-driven changes in precipitation are illustrated in figure 1. Given the proliferated CO_2 conditions, as the temperature rises, precipitation increases (figures 1(A) and (B)). The atmospheric radiative cooling caused by tropospheric warming in equation (9) explains the precipitation variation under equilibrium responses after quadrupling CO_2 concentration (figure 1(A)). This SLOW response also explains volcanic eruption responses injecting sulfate aerosols to the atmosphere (figure S2(D)). However, SLOW represents the overestimation relative to the simulation of 1pctCO2 and historical (figures 1(B) and (C)). The gap between simulation and SLOW is mostly transient RF effects (FAST), inhibiting a room for latent heat release resulting decrease in precipitation. It is noteworthy that equation (9) can capture both MME mean responses and the spread of ensemble members, proving the

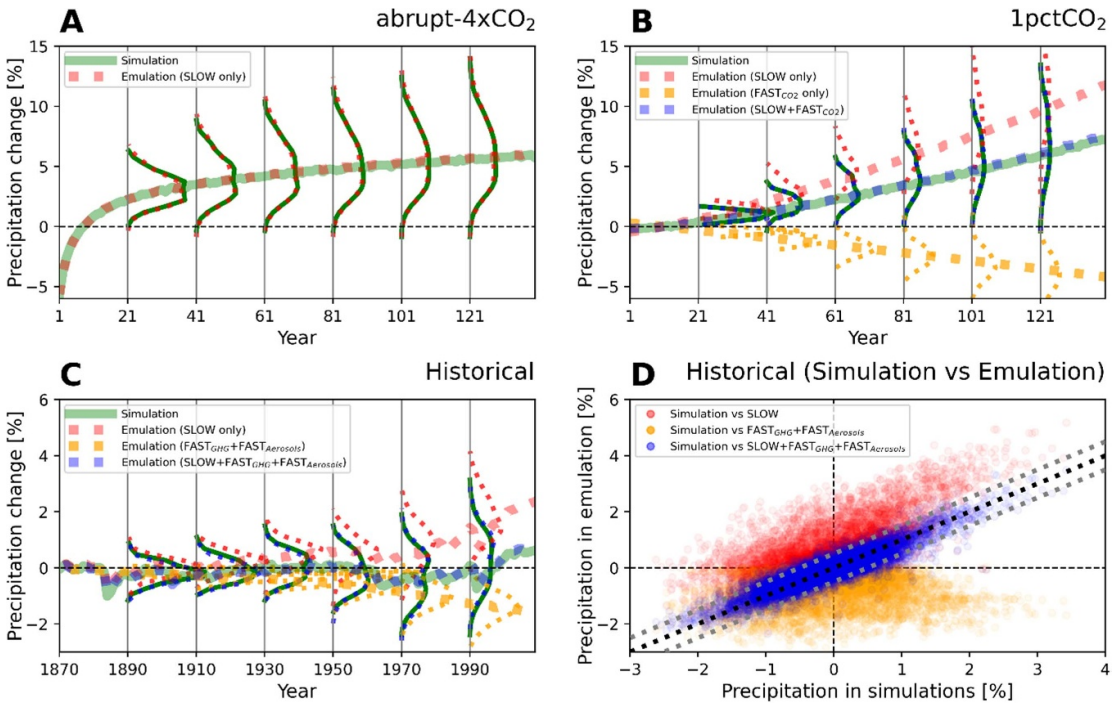

Figure 1. Global averaged annual mean precipitation changes relative to the first twenty years (1–20 years of abrupt-4xCO2 and 1pctCO2, and 1850–1869 years of historical). (A)–(C) The ensemble distribution of simulations (solid lines) and emulations (dashed lines) are shown vertically together after applying smoothing by kernel density estimation for every twenty years of chunks. Horizontally drawn solid and dashed lines represent the ensemble-averaged results of simulations and emulations. (D) Scatter plot between simulations and emulations of 55 GCMs for 165 historical years (1850–2014). Black and two grey diagonal lines indicate one-to-one reference and ±0.5% error ranges in emulations, respectively. The results of emulations are categorized as three: (A)–(D) only temperature effects (SLOW, red), (B)–(D) only atmospheric radiative effects ($FAST_{CO_2}$), or $FAST_{GHG} + FAST_{Aerosols}$, orange), and (B)–(D) the sum of these effects (SLOW + $FAST_{CO_2}$ or SLOW + $FAST_{GHG}$ + $FAST_{Aerosols}$, blue).

validity of our equation to capture precipitation variation (figures 1 and S2). To check the likely ranges of computation error between emulation and simulation, we draw the one-to-one scatter plot and reaffirm that error size is mainly within ±0.5% when all components are considered (figure 1(D)). We confirm emulations usually have the size of error less than 0.1% in climate sense (figure S4).

3.2. Contributions to forcing-driven precipitation change

Our equation can decompose the precipitation variation into two components: SLOW and FAST. FAST is divided into RF types (CO_2, CH_4, N_2O, and aerosols). We investigate their contributions to the MME mean and uncertainty in rainfall change (figure 2). Changes in the precipitation of simulations are reproduced reasonably by emulations (figures 1(C) and 2(A)). Our decomposition reveals that a tremendous amount of precipitation increases due to global warming is offset by RF in the atmosphere coupled with the anthropogenic components (figure 2(A)). The size of uncertainty among GCMs increases with time (figures 1(C) and 2(B)) as the increase in the variance of simulated temperature (figure S3(A)). In the last 20 years of historical periods (1995–2014), MME mean of simulations expect a 0.45% increase, and MME variance is around $0.95\%^2$. As MME mean is about half size of MME standard deviation, about 36% GCMs show negative changes (figure S4), suggesting a noticeable disagreement in precipitation trend under the historical experiment. The total variance is comparable to SV (figures 2(B) and S3(A)). We decompose SV with equation (15) (section 2.4) and manifest the quantified contributions from each component (figure 2(C)). The driving contributor is the temperature (SLOW ΔT), taking more than half of SV. The second largest contributor is $FAST_{Aerosols}$, reflecting the largest spread among parameters (table S3).

Similarly, we apply this equation to understand the precipitation changes under SSP scenarios (figure 3). These future results validate the reliability in our equaiton because most SSP emulations have an error size of less than 1% without updating any parameters (figure S5). Precipitation change are mainly driven by SLOW and offset by $FAST_{CO2}$ following the results of the historical period (figure 2(A)). Contrary to the historical case, the $FAST_{Aerosols}$ increase precipitation due to the decrease in aerosols concentration in all future scenarios (figures 3(A)–(C)). The size of SV in the late 21st Century (2081–2100) is 1.76, 2.47, and $6.99\%^2$ for SSP1-2.6, SSP2-4.5, and SSP5-8.5, emphasizing the larger uncertainty for the more

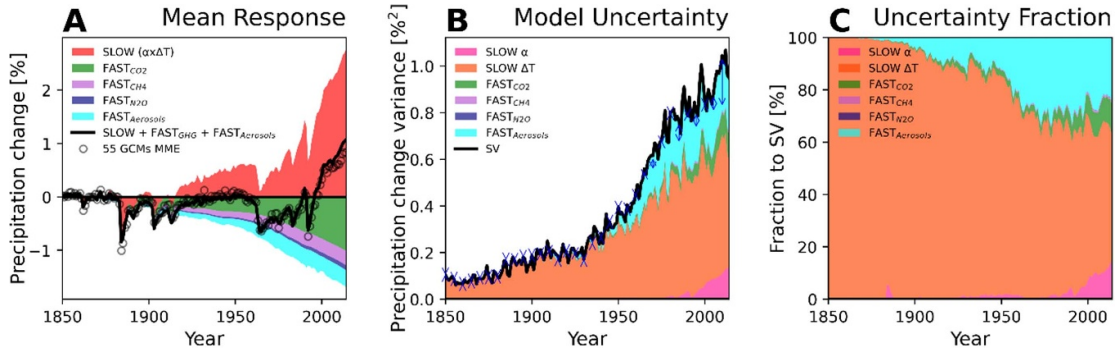

Figure 2. (A) Time-varying precipitation amount (%) relative to 1850–1869 years and its decomposed contribution from SLOW, $FAST_{GHG}$ (sum of $FAST_{CO2}$, $FAST_{CH4}$, and $FAST_{N2O}$), and $FAST_{Aerosols}$ with colors. The MME mean results of 55 simulations (open circles) and emulations (solid black line: sum of SLOW, $FAST_{GHG}$, and $FAST_{Aerosols}$) are shown together. (B) Time-varying size of uncertainty ($\%^2$) among emulations, decomposed by various components. The difference between the variance of precipitation and the sum of single variable effects (Sum of Variance, SV) are shown by arrows for every five years. This size represents the uncertainty from interactions between multiple variables (Cov, see equation (12) in section 2.4). (C) The relative uncertainty contribution size from components to SV is illustrated (Single variable effects/SV*100).

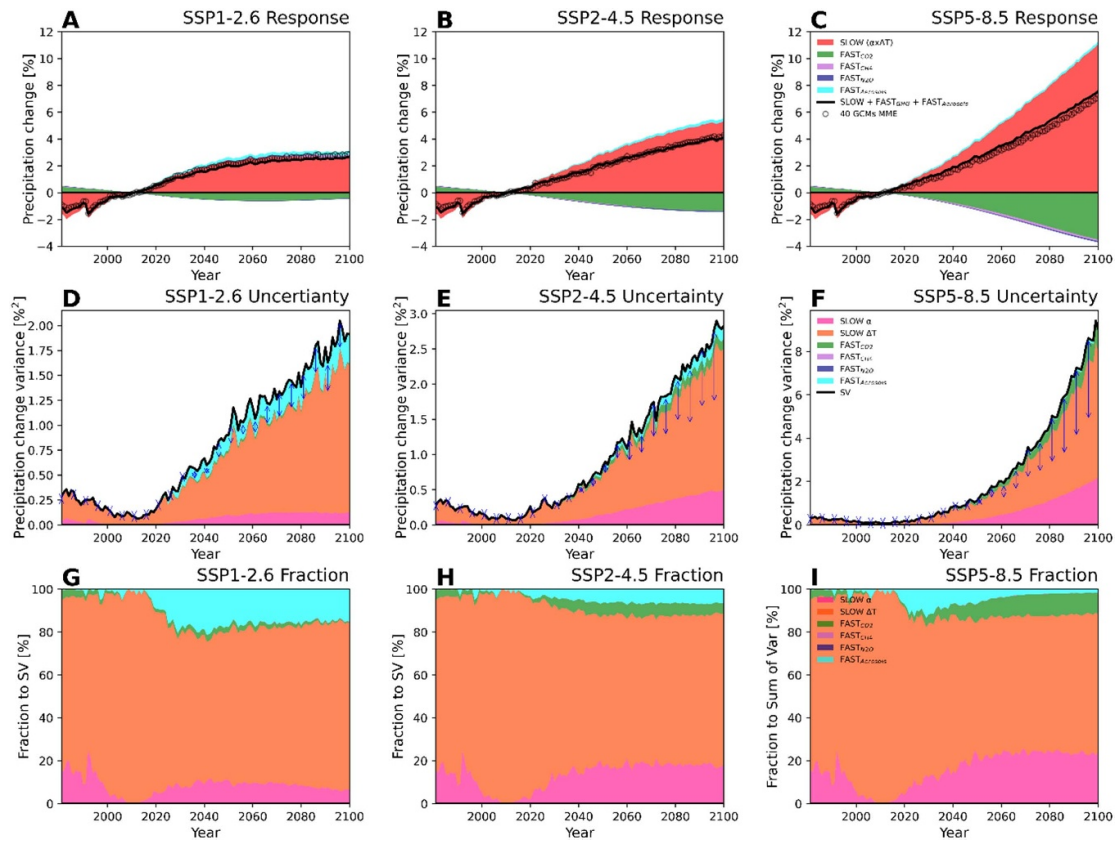

Figure 3. Same as figure 2, except for the future changes in precipitation relative to 2001–2020 years of 40 simulations and emulations under three SSP scenarios (SSP1-2.6, SSP2-4.5, and SSP5-8.5).

severe warming scenarios. Accordingly, SV primarily originates from SLOW (at leasts 80% for all SSP scenarios), highlighting noticeable model disagreement on the effects of global warming. While the size of uncertainty in $FAST_{Aerosols}$ is noticeable for the low-emission scenario, SSP1-2.6 (figure 3(D)), it is not vital for the high-emission scenario, SSP5-8.5, because the $FAST_{CO2}$ is much larger than $FAST_{Aerosols}$ (figure 3(F)). This characteristic is also reflected in the fraction of uncertainty (figures 3(G)–(I)).

3.3. Precipitation change at global warming mitigation pathways

Since the temperature change is the vital contributor to the mean response and uncertainty (figures 2 and 3), here we assess the statistically estimated

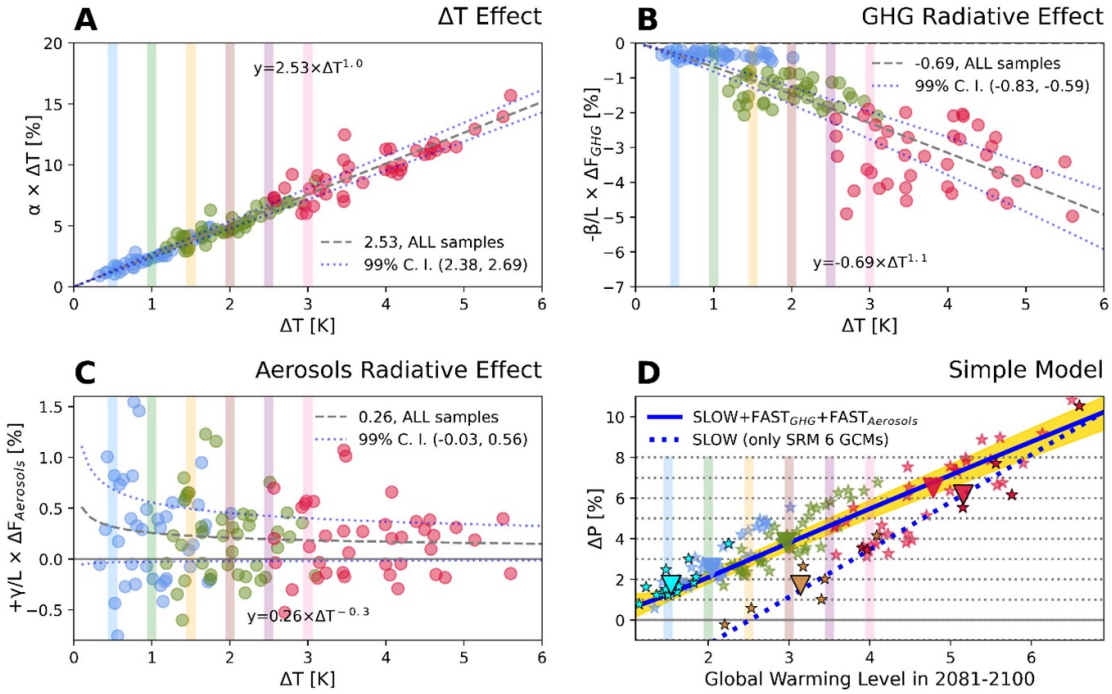

Figure 4. (A)–(C) Scatter plot between temperature changes and decomposed precipitation change (circle for each emulation) in 20 years (2081–2100) under three SSP scenarios (blue: SSP1-2.6, green: SSP2-4.5, and red: SSP5-8.5) relative to 20 years (2001–2020). Three different contributions and statistically fitted functions for them are shown for (A) temperature-driven radiative cooling, slow response (ΔT effect), and instantaneous radiative forcing effects driven by (B) GHG (GHG Radiative Effect) and (C) aerosols (Aerosols Radiative Effect). The optimized temperature-dependent functions are established from 120 samples (40 GCMs × 3 SSPs). The likely ranges of parameter slope (dotted lines, 0.5 and 99.5th percentile values) are estimated by the bootstrapping method. (D) The prediction for precipitation change from a simple model, combining three functions and slopes in (A)–(C). For the global warming level in 2081–2100, we reflect the observed warming level in the recent 20 years, 1.0 K (https://globalwarmingindex.org/), to the relative changes in temperature shown in (A)–(C). An asterisk denotes each result of the GCM simulation. The reversed triangles represent the MME mean of simulations under the corresponding scenarios. Solid lines and shading area indicate the best estimation and 99% confidence interval ranges, respectively, conditional on the specific warming levels under the GGR. As a validation of this simple model, SSP1-1.9 and SRM simulations are shown together (cyan: SSP1-1.9, 14 GCMs and brown: SRM, 6 GCMs), and their simulations are remarked with black outlines. The diagonal dotted line represents the best estimation conditional on the specific warming levels under SRM by considering their GCM members. For SSP5-8.5, the reversed triangle with outline indicates MME mean under SSP5-8.5 after selecting GCM members of SRM. (A)–(D) The relative warming levels in 20 years of the late 21st Century are illustrated by vertical lines with colors (+0.5, +1.0, +1.5, +2.0, +2.5, and +3.0 K, respectively).

ranges of precipitation changes conditional on the different global warming levels (figure 4). First, we built a function ($y = \text{slope} \times \Delta T^{\text{exponent}}$) finding the best relationship between decomposed equation (9) and global warming levels. We found the optimized parameters (slope and exponent) fitting with 120 samples (40 GCMs × 3 SSP scenarios) for SLOW, FAST_{GHG}, and $\text{FAST}_{\text{Aerosols}}$ components at the late 21st century. The optimized functions are $2.53\times\Delta T^{1.0}$, $-0.69\times\Delta T^{1.1}$, and $0.26\times\Delta T^{-0.2}$ for SLOW, FAST_{GHG}, and $\text{FAST}_{\text{Aerosols}}$, respectively. The ranges of the likely mean of emulations at specific warming levels can be measured statistically from a simple model, which is the sum of these functions. We obtain a 99% confidence interval (99% CI) from bootstrapping samples of alternative slope in each function with a half size of GCM members.

First, the estimated changes in precipitation caused by temperature, SLOW (figure 4(A)), are similar to the averaged parameter of 55 GCMs, 2.55%/K (table S3). Different GHG amount in three scenarios and small spread in parameter β (table S3) makes a statically sturdy relationship ($r = -0.80$) between global warming levels and FAST_{GHG} (figure 4(B)), illustrating the possible relationship between GHG RF amount and global warming levels. While, for the RF effects of aerosols, the estimated function is nearly constant due to the negligible differences in aerosols' effective RF of three scenarios and the sizeable inter-model spread in parameter γ (table S3). As a result, the function for the radiative effect of aerosols is much more sensitive to the member of models rather than global warming levels ($r = -0.10$).

Finally, this simple model predicts changes in precipitation under specific warming conditions under GGR and SRM (figure 4(D)). We reflect the observed anthropogenic warming level of 1.0 K in 2001–2020 (https://globalwarmingindex.org, Haustein *et al* 2017) to the relative warming levels in late 21st Century. All 120 simulations are positioned around the simple model. For validation, we compare 14 simulations of SSP1-1.9 which are not involved in optimizing functions but are located around the prediction of the simple model. About GGR, the reversed

contribution sign between $FAST_{GHG}$ and $FAST_{Aerosols}$ implies that aerosols would affect more than GHG in the specific range of temperatures (figures 4(B) and (C)). We compute this particular global warming level with the negative $FAST_{GHG}$ offsetting the positive $FAST_{Aerosols}$, resulting in no combined FAST contribution, which is about 1.5 K. Thus, the mitigation pathways below 1.5 K are more likely to be influenced by RF of aerosols than GHG. We also compare the estimated results of GGR and SRM together. Here, to calculate SRM prediction, we first select six GCMs having SRM experiments (table S1) and find their MME mean changes in temperature and precipitation under SSP5-8.5. Then we draw the lines crossing this MME mean only driven by the SLOW. This simple prediction is well around the SRM simulations, affirming drier conditions in SRM than GGR due to remaining atmospheric GHG radiative effects (MacMartin *et al* 2018, Laakso *et al* 2020, Visioni *et al* 2021, 2023).

Under the global warming mitigation plans of GGR according to the Paris Agreement (1.5 K or 2.0 K), our simple model predicts a precipitation increase of about 0.91 $\sim$ 1.62%, or 1.80 $\sim$ 2.39% (99% CI). All predictions from 1.1 to 4.0 K are summarized in table S4. Our simple model with optimized functions highlights that SRM effectively cools global warming but accompanies severe drought than GGR approaches. To check the robustness of our optimized functions, we examined the effects of different based periods on optimizing functions (table S5). We confirmed that each term of function is mostly invariant. However, watchfulness is required for the base periods after 2020 because aerosols and GHG emissions are heterogeneous in SSP scenarios (Lund *et al* 2019, Meinshausen *et al* 2020, Smith *et al* 2021), affecting statistical optimization.

4. Summary and discussion

This study introduces a physically based equation to examine changes in global mean precipitation under various scenarios having different mitigation pathways. The latent heat release by precipitation is balanced by SLOW and FAST, representing the temperature-dependent and temperature-independent change, respectively. After finding the three parameters of each GCM, the equation can capture both the mean and the spread of simulations. The decomposition of equation reveals that a tremendous amount of precipitation increase due to global warming is offset by RF in the atmosphere coupled with anthropogenic forcings. Since most uncertainty is derived from the disagreement in global warming levels, this study proposes a simple model predicting precipitation change based on the relationship between each term of our equation and global warming levels. This simple model reveals that the size of aerosols' RF is critical for precipitation change around 1.5 K. Based on the physically based characteristics of GGR and SRM, we compare the results from different mitigation approaches, and our simple model physically proves the drier conditions in SRM than the GGR.

Our results are broadly consistent with previous studies analyzing the global mean precipitation changes under future scenarios of CMIP Phase 5 (Caesar *et al* 2013, Hegerl *et al* 2015), CMIP6 (Tebaldi *et al* 2021), and SRM (MacMartin *et al* 2018, Laakso *et al* 2020, Visioni *et al* 2021, 2023). A simple model uncovers the nonlinearity in precipitation increase to global warming levels originating from $FAST_{GHG}$ corresponding to the results of various GCM experiments (e.g. Mitchel *et al* 2016, Salzmann 2016, Li *et al* 2019). This simple equation can explain the higher slope of total precipitation response conditional on total temperature change for low-emission than high-emission scenarios (Hegerl *et al* 2015). The most considerable fraction of precipitation uncertainty is from the disagreement in global warming levels, supporting the findings of Fläschner *et al* (2016). HS in CMIP6 has less bias than it in CMIP5, possessing bias in cloud interaction (Watanabe *et al* 2018), according to the anti-correlated relationship between equilibrium climate sensitivity and HS (Watanabe *et al* 2018, Pendergrass 2020, Ribes *et al* 2021). We expect a simple climate model (e.g. Smith *et al* 2018) can employ our equation, and this employment enables the prevision of precipitation variations under various future scenarios, much more effectively than complex climate models. These theoretical foresights can impress policymakers, such as the importance of redeeming a pledge to implement mitigation pathways aimed at the Paris Agreement.

Nonetheless, caveats remain in our study. First, our emulations cannot reproduce the precipitation variation on annual and decadal scales (figure S3). Reflection of the natural variability to the emulations will diminish the errors (e.g. Lenssen *et al* 2020). Second, our parameters are concisely defined but have further uncertainty sources that should be explored, such as ocean warming patterns effects (e.g. Zhang *et al* 2023), different characteristics in aerosols' sub-component (Richardson *et al* 2018, Zhang *et al* 2021), and model structure or component effects (e.g. Qian *et al* 2018, Tett *et al* 2022). Third, the simple prediction model for GGR is statistically designed with assumptions on linear-like forcing conditions between SSP scenarios. Our following study will examine dynamical climate model simulations under the adaptive emission scenarios (Terhaar *et al* 2022) to check the validity of the statistical assumption. The next goal of our equation is to resolve the mathematization of different responses over land and ocean.

Data availability statement

The CMIP6 model data sets that support the findings of this study are openly available at https://esgf-node.llnl.gov/projects/cmip6/. All data that support the findings of this study are included within the article (and any supplementary files).

Acknowledgments

We acknowledge two anonymous reviewers for their constructive comments that improved this manuscript. We acknowledge the World Climate Research Programme, which, through its Working Group on Coupled Modeling, coordinated and promoted CMIP6. We acknowledge the climate modeling groups for producing and making available their model output, the Earth System Grid Federation (ESGF) for archiving the data and providing access, and the multiple funding agencies who support CMIP6 and ESGF. This work used JASMIN, the UK collaborative data analysis facility. This project has received funcing from the European Union's Horizon 2020 research and innovation programme (4C project, Grant Agreement No. 821003) (D L, M R A). S W Y was supported by Korea Environment Industry and Technology Institute (KEITI) through-Climate Change R&D Project for New Climate Regime funded by Korea Ministry of Environment (MOE) (2022003560001).

ORCID iDs

Donghyun Lee https://orcid.org/0000-0003-0184-2712
Sarah N Sparrow https://orcid.org/0000-0002-1802-6909
Seung-Ki Min https://orcid.org/0000-0002-6749-010X
Sang-Wook Yeh https://orcid.org/0000-0003-4549-1686
Myles R Allen https://orcid.org/0000-0002-1721-7172

References

Abramowitz G, Herger N, Gutmann E, Hammerling D, Knutti R, Leduc M, Lorenz R, Pincus R and Schmidt G A 2019 ESD reviews: model dependence in multi-model climate ensembles: weighting, sub-selection and out-of-sample testing *Earth Syst. Dyn.* **10** 91–105

Allen M R and Ingram W J 2002 Constraints on future changes in climate and the hydrologic cycle *Nature* **419** 224–32

Andrews T, Gregory J M and Webb M J 2015 The dependence of radiative forcing and feedback on evolving patterns of surface temperature change in climate models *J. Clim.* **28** 1630–48

Bengtsson L 2010 The global atmospheric water cycle *Environ. Res. Lett.* **5** 025202

Caesar J, Palin E, Liddicoat S, Lowe J, Burke E, Pardaens A, Sanderson M and Kahana R 2013 Response of the HadGEM2 Earth system model to future greenhouse gas emissions pathways to the year 2300* *J. Clim.* **26** 3275–84

Etminan M, Myhre G, Highwood E J and Shine K P 2016 Radiative forcing of carbon dioxide, methane, and nitrous oxide: a significant revision of the methane radiative forcing *Geophys. Res. Lett.* **43** 12614–23

Fläschner D, Mauritsen T and Stevens B 2016 Understanding the intermodel spread in global-mean hydrological sensitivity* *J. Clim.* **29** 801–17

Gleeson T *et al* 2020 Illuminating water cycle modifications and Earth system resilience in the anthropocene *Water Resour. Res.* **56** e2019WR024957

Haustein K, Allen M R, Forster P M, Otto F E L, Mitchell D M, Matthews H D and Frame D J 2017 A real-time global warming index *Sci. Rep.* **7** 15417

Hawkins E and Sutton R 2009 The potential to narrow uncertainty in regional climate predictions *Bull. Am. Meteorol. Soc.* **90** 1095–108

Hawkins E and Sutton R 2011 The potential to narrow uncertainty in projections of regional precipitation change *Clim. Dyn.* **37** 407–18

Hegerl G C *et al* 2015 Challenges in quantifying changes in the global water cycle *Bull. Am. Meteorol. Soc.* **96** 1097–115

Held I M and Soden B J 2006 Robust responses of the hydrological cycle to global warming *J. Clim.* **19** 5686–99

Hirabayashi Y, Mahendran R, Koirala S, Konoshima L, Yamazaki D, Watanabe S, Kim H and Kanae S 2013 Global flood risk under climate change *Nat. Clim. Change* **3** 816–21

Kriegler E, Luderer G, Bauer N, Baumstark L, Fujimori S, Popp A, Rogelj J, Strefler J and Van Vuuren D P 2018 Pathways limiting warming to 1.5 °C: a tale of turning around in no time? *Phil. Trans. R. Soc.* A **376** 20160457

Kundzewicz Z W and Döll P 2009 Will groundwater ease freshwater stress under climate change? *Hydrol. Sci. J.* **54** 665–75

Laakso A, Snyder P K, Liess S, Partanen A-I and Millet D B 2020 Differing precipitation response between solar radiation management and carbon dioxide removal due to fast and slow components *Earth Syst. Dyn.* **11** 415–34

Lee D S *et al* 2021 The contribution of global aviation to anthropogenic climate forcing for 2000–2018 *Atmos. Environ.* **244** 117834

Lee D, Min S-K, Ahn J-B, Cha D-H, Shin S-W, Chang E-C, Suh M-S, Byun Y-H and Kim J-U 2023 Uncertainty analysis of future summer monsoon duration and area over East Asia using a multi-GCM/multi-RCM ensemble *Environ. Res. Lett.* **18** 064026

Lehner F, Deser C, Maher N, Marotzke J, Fischer E M, Brunner L, Knutti R and Hawkins E 2020 Partitioning climate projection uncertainty with multiple large ensembles and CMIP5/6 *Earth Syst. Dyn.* **11** 491–508

Lenssen N J L, Goddard L and Mason S 2020 Seasonal forecast skill of ENSO teleconnection maps *Weather Forecast.* **35** 2387–406

Li Z, Sun Y, Li T, Ding Y and Hu T 2019 Future changes in East Asian Summer Monsoon Circulation and precipitation under 1.5–5 °C of warming *Earth's Future* **7** 1391–406

Lund M T, Myhre G and Samset B H 2019 Anthropogenic aerosol forcing under the shared socioeconomic pathways *Atmos. Chem. Phys.* **19** 13827–39

MacMartin D G, Ricke K L and Keith D W 2018 Solar geoengineering as part of an overall strategy for meeting the 1.5 °C Paris target *Phil. Trans. R. Soc.* A **376** 20160454

Meinshausen M *et al* 2020 The shared socio-economic pathway (SSP) greenhouse gas concentrations and their extensions to 2500 *Geosci. Model Dev.* **13** 3571–605

Mitchell D, James R, Forster P M, Betts R A, Shiogama H and Allen M 2016 Realizing the impacts of a 1.5 °C warmer world *Nat. Clim. Change* **6** 735–7

Myhre G *et al* 2018 Quantifying the importance of rapid adjustments for global precipitation changes *Geophys. Res. Lett.* **45** 11–399

Myhre G, Highwood E J, Shine K P and Stordal F 1998 New estimates of radiative forcing due to well mixed greenhouse gases *Geophys. Res. Lett.* **25** 2715–8
Nguyen T-H, Min S-K, Paik S and Lee D 2018 Time of emergence in regional precipitation changes: an updated assessment using the CMIP5 multi-model ensemble *Clim. Dyn.* **51** 3179–93
Nicholls Z R J *et al* 2020 Reduced complexity model intercomparison project phase 1: introduction and evaluation of global-mean temperature response *Geosci. Model Dev.* **13** 5175–90
Paik S, Min S, Zhang X, Donat M G, King A D and Sun Q 2020 Determining the anthropogenic greenhouse gas contribution to the observed intensification of extreme precipitation *Geophys. Res. Lett.* **47** e2019GL086875
Pendergrass A G 2020 The global-mean precipitation response to CO_2 -induced warming in CMIP6 models *Geophys. Res. Lett.* **47** e2020GL089964
Qian Y *et al* 2018 Parametric sensitivity and uncertainty quantification in the version 1 of E3SM atmosphere model based on short perturbed parameter ensemble simulations *J. Geophys. Res. Atmos.* **123** 13–46
Ribes A, Qasmi S and Gillett N P 2021 Making climate projections conditional on historical observations *Sci. Adv.* **7** eabc0671
Richardson T B *et al* 2018 Drivers of precipitation change: an energetic understanding *J. Clim.* **31** 9641–57
Richardson T B, Forster P M, Andrews T and Parker D J 2016 Understanding the rapid precipitation response to CO_2 and aerosol forcing on a regional scale *J. Clim.* **29** 583–94
Rugenstein M *et al* 2020 Equilibrium climate sensitivity estimated by equilibrating climate models *Geophys. Res. Lett.* **47** e2019GL083898
Salzmann M 2016 Global warming without global mean precipitation increase? *Sci. Adv.* **2** e1501572
Samset B H *et al* 2016 Fast and slow precipitation responses to individual climate forcers: a PDRMIP multimodel study *Geophys. Res. Lett.* **43** 2782–91
Sanderson B M *et al* 2017 Community climate simulations to assess avoided impacts in 1.5 and 2 °C futures *Earth Syst. Dyn.* **8** 827–47
Shine K P, Allan R P, Collins W J and Fuglestvedt J S 2015 Metrics for linking emissions of gases and aerosols to global precipitation changes *Earth Syst. Dyn.* **6** 525–40
Smith C J *et al* 2020 Effective radiative forcing and adjustments in CMIP6 models *Atmos. Chem. Phys.* **20** 9591–618
Smith C J *et al* 2021 Energy budget constraints on the time history of aerosol forcing and climate sensitivity *Geophys. Res. Atmos.* **126** e2020JD033622
Smith C J, Forster P M, Allen M, Leach N, Millar R J, Passerello G A and Regayre L A 2018 FAIR v1.3: a simple emissions-based impulse response and carbon cycle model *Geosci. Model Dev.* **11** 2273–97
Smith C 2020 Effective radiative forcing time series from the shared socioeconomic pathways (available at: https://zenodo.org/record/3973015)
Tebaldi C *et al* 2021 Climate model projections from the scenario model intercomparison project (ScenarioMIP) of CMIP6 *Earth Syst. Dyn.* **12** 253–93
Terhaar J, Frölicher T L, Aschwanden M T, Friedlingstein P and Joos F 2022 Adaptive emission reduction approach to reach any global warming target *Nat. Clim. Change* **12** 1136–42
Tett S F B, Gregory J M, Freychet N, Cartis C, Mineter M J and Roberts L 2022 Does model calibration reduce uncertainty in climate projections? *J. Clim.* **35** 2585–602
Visioni D *et al* 2021 Identifying the sources of uncertainty in climate model simulations of solar radiation modification with the G6sulfur and G6solar geoengineering model intercomparison project (GeoMIP) simulations *Atmos. Chem. Phys.* **21** 10039–63
Visioni D *et al* 2023 Opinion: the scientific and community-building roles of the geoengineering model intercomparison project (GeoMIP)—past, present, and future *Atmos. Chem. Phys.* **23** 5149–76
Walther G-R, Post E, Convey P, Menzel A, Parmesan C, Beebee T J C, Fromentin J-M, Hoegh-Guldberg O and Bairlein F 2002 Ecological responses to recent climate change *Nature* **416** 389–95
Watanabe M, Kamae Y, Shiogama H, DeAngelis A M and Suzuki K 2018 Low clouds link equilibrium climate sensitivity to hydrological sensitivity *Nat. Clim. Change* **8** 901–6
Ya Kondratev K 1972 *Radiation Processes in the Atmosphere* (World Meteorological Organization)
Yeh S-W, Song S-Y, Allan R P, An S-I and Shin J 2021 Contrasting response of hydrological cycle over land and ocean to a changing CO_2 pathway *npj Clim. Atmos. Sci.* **4** 53
Yip S, Ferro C A T, Stephenson D B and Hawkins E 2011 A simple, coherent framework for partitioning uncertainty in climate predictions *J. Clim.* **24** 4634–43
Zelinka M D, Andrews T, Forster P M and Taylor K E 2014 Quantifying components of aerosol-cloud-radiation interactions in climate models *J. Geophys. Res. Atmos.* **119** 7599–615
Zhang S, Stier P, Dagan G, Zhou C and Wang M 2023 Sea surface warming patterns drive hydrological sensitivity uncertainties *Nat. Clim. Change* **13** 545–53
Zhang S, Stier P and Watson-Parris D 2021 On the contribution of fast and slow responses to precipitation changes caused by aerosol perturbations *Atmos. Chem. Phys.* **21** 10179–97
Zhou Y and Savijärvi H 2014 The effect of aerosols on long wave radiation and global warming *Atmos. Res.* **135–136** 102–11